

A Hybrid Eulerian-Eulerian Discrete-Phase Model of Turbulent Bubbly Flow

Hyunjin Yang

Department of Mechanical Science and Engineering,
University of Illinois at Urbana-Champaign
1206 W. Green Street, Urbana, IL 61801 USA
hyang69@illinois.edu

Surya P. Vanka¹

Department of Mechanical Science and Engineering,
University of Illinois at Urbana-Champaign
1206 W. Green Street, Urbana, IL 61801 USA
spvanka@illinois.edu
ASME Fellow

Brian G. Thomas

Department of Mechanical Engineering,
Colorado School of Mines
Brown Hall W370-B, 1610 Illinois Street, Golden, CO 80401 USA
bgthomas@csm.edu

ABSTRACT

The Eulerian-Eulerian two-fluid model (EE) [1] is a powerful general model for multiphase flow computations. However, one limitation of the EE model is that it has no ability to estimate the local bubble sizes by itself. Thus, it must be complemented either by measurements of bubble size distribution or by additional models such as population balance theory or interfacial area concentration to get the local bubble size information. In this work, we have combined the Discrete Phase model (DPM) [2] to estimate the evolution of bubble sizes with the Eulerian-Eulerian model. In the DPM, the bubbles are tracked individually as point masses, and the change of bubble size distribution is estimated by additional coalescence and breakup modeling of the bubbles. The time-varying bubble distribution is used to compute the local interface

¹ Corresponding author.

area between gas and liquid phase, which is then used to estimate the momentum interactions such as drag, lift, wall lubrication and turbulent dispersion forces for the EE model. In this work, this newly-developed hybrid model (EEDPM) is applied to compute an upward flowing bubbly flow in a vertical pipe and the results are compared with previous experimental work of Hibiki et al. [3]. The EEDPM model is able to reasonably predict the locally different bubble size distributions and the velocity and gas fraction fields. On the other hand, the standard EE model without the DPM shows good comparison with measurements only when the prescribed constant initial bubble size is accurate and does not change much. Parametric studies are implemented to understand the contributions of bubble interactions and volumetric expansion on the size change of bubbles quantitatively. The results show that pressure expansion is significant. However, coalescence is larger than other effects, and naturally increases in importance with increasing gas fraction.

INTRODUCTION

Analysis of multiphase flow systems has received great attention as a grand challenge problem in Computational Fluid Dynamics (CFD) due to its importance for a wide variety of industrial processes (cooling, energy generation, material processing, chemical reactions etc.). In spite of numerous studies to date, the modeling of liquid-gas systems is still difficult due to its complexity and lack of fundamental understanding. The Eulerian-Eulerian (EE) model has been demonstrated to provide some success in simulating practical multiphase flow problems. However, the accuracy of this model is limited by the absence of reliable models for interphase coupling. EE models require additional help from measurements or additional modeling of interfacial coupling such as bubble characteristics (size, shape and so on) to calculate momentum interactions.

The present paper specifically addresses multiphase flows in the bubbly and transition regime to slug flow. Here we have combined and improved a model for the bubbly flow regime within the Eulerian-Eulerian model. One of the uncertainties in bubbly-EE models is the bubble size distribution. Previous works show that there are several approaches to analyze the evolution of bubble size distribution. One of the most popular approaches, especially in the chemical engineering field, is Population Balance Theory (PBT) [4]. In this model, a transport equation is solved for the number density of bubbles for each bubble size in addition to solving the EE model, which consists of at least two sets of continuity and momentum equations. Coalescence and breakup effects are modeled as source terms in the number density transport equation as birth and death rates. Numerous works have been published to close these source terms. A difficulty of using PBT in practical industrial problems is the high computational cost as the number density transport equation is a complex integro-differential equation, and governing equations must be solved for several bubble sizes. Several other models have been developed alleviate this issue: 1) Multi-size group (MUSIG) models [5-6] reduce the number of tracked bubble sizes by predefining them as a discrete distribution at input, 2) Interfacial Area Concentration (IAC) models [7] express the bubble distribution as interface area of bubbles and tracks it by solving a transport equation for the interface area instead of the number density. A major limitation of the MUSIG model is predefining the range of discrete bubble sizes as bubble interactions are estimated only for the prefixed finite bubble sizes. Therefore, this model relies on intuition to determine the bubble size ranges, and the result is dependent on the choice. With IAC models, the

bubble size obtained from the IAC model is a locally averaged (Sauter-mean) bubble size. Hence, it is not possible to evaluate the bubble size distribution. Also, this model is difficult to apply for new fluids as it requires many empirical constants.

In contrast with these Eulerian-based approaches, there are discrete approaches using Lagrangian point-particle tracking, called Discrete Phase Models (DPM) [8]. With DPM, each particle making up the discrete phase is tracked individually as a point mass using Newton's equations of motion. Based on the interaction with a continuous phase, it is classified to be one-way coupled (only the continuous phase affects the discrete phase) or two-way coupled (both phases interact with each other). Recently, four-way coupled simulations have also been introduced by including particle-particle interactions such as collisions, coalescence and breakup [9]. This approach allows simulation of high gas volume fraction bubbly flows. A weakness of DPM is that a Lagrangian point-particle is not suitable to represent large bubbles ($d \gg x$) such as Taylor bubbles or gas pockets formed by accumulation of bubbles in recirculation zones.

Recently we have [10] combined a discrete approach for estimating the evolution of bubble sizes with a Eulerian-Eulerian model: the evolution of bubble size distribution is captured by DPM, and the bubble size information is used to calculate local momentum interactions in the EE model. In this paper, this model is applied in an upward-flowing bubbly flow in a vertical pipe and the results are validated against previous experimental work of Hibiki et al. (2001) [3].

MODEL DESCRIPTION: GOVERNING EQUATIONS

The current model solves the following equations for the liquid and gas phases.

$$\frac{\partial(\alpha_g \rho_g)}{\partial t} + \nabla \cdot (\alpha_g \rho_g \mathbf{u}_g) = 0 \quad (1)$$

$$\frac{\partial(\alpha_l \rho_l)}{\partial t} + \nabla \cdot (\alpha_l \rho_l \mathbf{u}_l) = 0 \quad (2)$$

$$\begin{aligned} & \frac{\partial(\alpha_g \rho_g \mathbf{u}_g)}{\partial t} + \nabla \cdot (\alpha_g \rho_g \mathbf{u}_g \mathbf{u}_g) \\ &= -\alpha_g \nabla p + \nabla \cdot (\mu_g \alpha_g (\nabla \mathbf{u}_g + \nabla \mathbf{u}_g^T)) + \alpha_g \rho_g \mathbf{g} + \sum \mathbf{F}_g \end{aligned} \quad (3)$$

$$\begin{aligned} & \frac{\partial(\alpha_l \rho_l \mathbf{u}_l)}{\partial t} + \nabla \cdot (\alpha_l \rho_l \mathbf{u}_l \mathbf{u}_l) \\ &= -\alpha_l \nabla p + \nabla \cdot (\mu_l \alpha_l (\nabla \mathbf{u}_l + \nabla \mathbf{u}_l^T)) + \alpha_l \rho_l \mathbf{g} + \sum \mathbf{F}_l \end{aligned} \quad (4)$$

$$\rho_g V_p \frac{dv_i}{dt} = V_c \sum \mathbf{F}_g + \mathbf{F}_B \quad (5)$$

$$\frac{dx_i}{dt} = \mathbf{v}_i \quad (6)$$

$$\begin{aligned} \sum \mathbf{F}_l &= -\sum \mathbf{F}_g \\ &= \mathbf{F}_D + \mathbf{F}_L + \mathbf{F}_W + \mathbf{F}_T + \mathbf{F}_V + \mathbf{F}_P \end{aligned} \quad (7)$$

As the name of the model suggests, the governing equations are composed of two parts: the EE model has two continuity equations (Eq. 1-2) and six momentum equations (Eq. 3-4) for the two phases to calculate velocity and volume fraction fields of each phase and a shared pressure field. The DPM equations (Eq. 5-6) track each bubble as a point-mass and store its position, velocity and acceleration. The two models are run together as separate models in the same domain, but are coupled by calculating $\sum \mathbf{F}_g$ for the DPM bubbles using the Eulerian liquid phase flow field. The DPM bubbles do not affect the liquid phase

field directly, but the DPM bubble size distribution influences the calculation of the EE model momentum interactions $\sum \mathbf{F}_l$ and $\sum \mathbf{F}_g$ by transferring the DPM bubble sizes to the EE model. Since this will change the liquid phase flow field in the end, this model is a semi-two-way coupled in one sense. It is important to decide which model is used for modeling momentum interaction terms (Eq. 7). Based on previous works [11,12], each force is modeled as follows. For calculating $\sum \mathbf{F}_g$ terms for the DPM equation (Eq. 5), the gas phase velocity \mathbf{u}_g is substituted to an individual bubble velocity \mathbf{v}_i , and α_g becomes 1 in these models.

For the drag force in the DPM model, the Tomiyama drag model [13] is chosen. This model considers deformation of bubble shape by including the Eotvos number EO in the drag coefficient calculation. Thus, it can be applied to a wide range of bubble shape regimes such as spherical, ellipsoidal and spherical caps. The drag law is given as

$$\mathbf{F}_D = -\frac{3}{4} \frac{C_D}{d} \rho_l \alpha_g |\mathbf{u}_g - \mathbf{u}_l| (\mathbf{u}_g - \mathbf{u}_l) \quad (8)$$

$$C_D = \max \left(\min \left(\frac{24}{Re_p} (1 + 0.15 Re_p^{0.687}), \frac{72}{Re_p} \right), \frac{8}{3} \frac{EO}{EO+4} \right) \quad (9)$$

where,

$$EO = \frac{g(\rho_l - \rho_g)d^2}{\sigma}, \quad Re_p = \frac{\rho_l |\mathbf{u}_g - \mathbf{u}_l| d}{\mu_l} \quad (10)$$

The lift force is important for lateral migration of bubbles. It is known that bubbles migrate differentially depending on their size. Large bubbles have more chance to be deformed due to their smaller surface tension forces and the substantial deformation

changes the lift force direction. The Tomiyama lift model [14] captures this sign inversion of lift force at bubble diameter $d=5.8\text{mm}$ based on the bubble shape through the Eotvos number.

$$\mathbf{F}_L = -C_L \rho_l \alpha_g (\mathbf{u}_g - \mathbf{u}_l) \times (\nabla \times \mathbf{u}_l) \quad (11)$$

$$C_L = \min[0.288 \tanh(0.121 Re_p), f(Eo')] \quad (Eo' \leq 4)$$

$$= f(Eo') \quad (4 < Eo' \leq 10)$$

$$= -0.27 \quad (10 < Eo') \quad (12)$$

where,

$$Eo' = \frac{g(\rho_l - \rho_g)d_h^2}{\sigma}, \quad d_h = d(1 + 0.163 Eo^{0.757})^{\frac{1}{3}} \quad (13)$$

$$f(Eo') = 0.00105 Eo'^3 - 0.0159 Eo'^2 - 0.0204 Eo' + 0.474 \quad (14)$$

However, Hibiki et al. (2001) [3] observed that this sign inversion happens when the bubble size becomes $d=3.6\text{mm}$, not $d=5.8\text{mm}$ in a multi-bubble situation. In this study, this lift force model is modified to match this observation by shifting the Tomiyama lift coefficient, C_L , as shown in Figure 1.

A wall lubrication force [15] is introduced to account for hydrodynamic forces near the wall. Basically this force always pushes bubbles away from the wall so that bubbles are kept detached from the wall. For small bubbles, the wall lubrication force acts in opposite direction to the lift force: the balance between these lateral forces, i.e. lift and wall lubrication forces plays a key role in determining the radial gas fraction profile.

$$\mathbf{F}_W = C_{WL} \rho_l \alpha_g |\mathbf{u}_g - \mathbf{u}_l|^2 \mathbf{n}_W \quad (15)$$

$$C_{WL} = \frac{C_W d}{2} \left(\frac{1}{y_w} \frac{1}{(D - y_w)^2} \right) \quad (16)$$

$$C_W = \max \left(\frac{7}{Re_p^{1.9}}, 0.0217 Eo \right) \quad (17)$$

A turbulent dispersion force [16] is also included to consider a force from turbulent fluctuations. Berns et al. derived this force through the Favre average of drag force. Numerically, this force smoothes out the gas fraction field.

$$\mathbf{F}_{T,l} = -\mathbf{F}_{T,g} = -\frac{3}{4} \frac{C_D}{d} \alpha_g |\mathbf{u}_g - \mathbf{u}_l| \frac{\mu_{t,l}}{\sigma_{lg}} \left(\frac{\nabla \alpha_g}{\alpha_g} - \frac{\nabla \alpha_l}{\alpha_l} \right) \quad (18)$$

The effect of bubbles on the turbulence of the liquid phase is modeled as a source term of turbulent viscosity [17].

$$\mu_{t,l} = C_{\mu,l} \frac{k_l^2}{\varepsilon_l} + 0.6 \alpha_g d |\mathbf{u}_g - \mathbf{u}_l| \quad (19)$$

For transient forces, the virtual mass force \mathbf{F}_V and pressure gradient force \mathbf{F}_P are added [17-18]. The virtual mass force (Eq. 20) is an additional force required to accelerate the surrounding fluid when the bubble is accelerated. The pressure gradient force (Eq. 21) arises when there is a nonuniform pressure distribution around the bubble.

$$\mathbf{F}_V = 0.5 \alpha_g \rho_l \left(\frac{D\mathbf{u}_l}{Dt} - \frac{D\mathbf{u}_g}{Dt} \right) \quad (20)$$

$$\mathbf{F}_P = \alpha_g \rho_l \frac{D\mathbf{u}_l}{Dt} \quad (21)$$

Most importantly, the buoyancy force for a DPM bubble is calculated as follows.

$$\mathbf{F}_B = \mathbf{g}(\rho_g - \rho_l) \quad (22)$$

VOLUMETRIC EXPANSION

Gas bubbles expand as they rise according to the surrounding liquid pressure field. To calculate the bubble size change due to liquid pressure changes, a cubic equation with respect to r_{new} (new bubble radius) is derived from the Young-Laplace equation and the ideal gas law:

$$p_{l,new} \left(\frac{d_{new}}{2} \right)^3 + 2\sigma \left(\frac{d_{new}}{2} \right)^2 - p_{g,old} \left(\frac{d_{old}}{2} \right)^3 = 0 \quad (23)$$

By solving this equation in time for the size of each DPM bubble, the gas volume change from the liquid pressure change is taken into account.

BUBBLE INTERACTION MODELING

Existing models for bubble breakup and coalescence are mostly developed in the framework of Population Balance Theory (PBT). Since bubbles are expressed with an Eulerian description in PBT, a suitable adjustment is required to transform these theories to a Lagrangian framework for applying them to DPM bubbles. Through this process, the complex integro-differential equations in PBT are simplified to ordinary differential

equations and algebraic equations, which are more intuitive and computationally inexpensive.

In the coalescence model, the collision frequency in PBT is easily handled from the calculation of distances between a pair of DPM bubbles. Here, only the distances between pairs located in the same computational cell are calculated to decrease the computational cost from n^2 to n (n = number of bubbles). Once the distance between the pair is smaller than the sum of the radii of two bubbles, the pair is counted as a collided pair. And then, the coalescence efficiency e is estimated through calculations of drainage time and contact time. According to Prince and Blanch, the drainage time ($t_{drainage}$) for the liquid film that forms between the collided pair and the contact time ($t_{contact}$) of the pair are calculated as follows [19]:

$$e = \exp\left(-\frac{t_{drainage}}{t_{contact}}\right) \quad (24)$$

$$t_{drainage} = \left[\frac{d_{eq}^3 \rho_l}{128\sigma}\right]^{0.5} \ln\left(\frac{h_i}{h_f}\right) \quad (25)$$

$$t_{contact} = \frac{(d_{eq}/2)^{\frac{2}{3}}}{\varepsilon^{\frac{1}{3}}} \quad (26)$$

$$d_{eq} = \frac{2}{1/d_1 + 1/d_2} \quad (27)$$

Coalescence efficiency e determines the probability of coalescence: if two bubbles merge, the coalesced bubble size and velocity are determined by mass and momentum conservation. Otherwise, the two bubbles bounce apart via an elastic collision. This is

reasonable assumption for small bubbles: strong surface tension makes bubbles behave as hard spheres. Our first trial with this approach caused over-estimation of coalescence since the contact time becomes too large due to low turbulent dissipation rate except near the wall. We could obtain a reasonable result with $e = 10^{-2}$. A more accurate model for coalescence efficiency is required in the future.

For the breakup model, the works of Luo & Svendsen [20] and Wang et al. [21] are chosen. In Luo and Svendsen's theory, a bubble breaks up when it meets an eddy that has smaller size than the bubble [22], but enough kinetic energy to create a new surface caused by breakup. To decide which eddy size hits a bubble, an eddy size is randomly determined in the range of $\lambda_{min} < \lambda < \lambda_{max}$ based on the eddy size distribution function. In Luo and Svendsen's work, the eddy size distribution is derived from the number density

of eddy $n_\lambda d\lambda = \frac{c_3(1-\alpha_g)}{\lambda^4} d\lambda$:

$$F(\lambda) = \frac{\text{number density of eddy that has size } \lambda_{min} \sim \lambda}{\text{total number density of eddies}}$$

$$= \frac{\int_{\lambda_{min}}^{\lambda} n_\lambda d\lambda}{\int_{\lambda_{min}}^{\lambda_{max}} n_\lambda d\lambda} = \frac{\lambda_{max}^3 \lambda_{min}^3}{\lambda_{max}^3 - \lambda_{min}^3} \left(\frac{1}{\lambda^3} - \frac{1}{\lambda_{min}^3} \right) \quad (28)$$

$$\lambda_{max} = \frac{D}{6}, \lambda_{min} = 11.4 \times \eta \quad (29)$$

Here, λ_{max} and λ_{min} stand for the maximum and minimum eddy sizes in the inertial subrange since the number density expression is derived under an assumption of isotropic turbulence in inertial subrange. Once an eddy size is determined randomly with the

cumulative probability density function $F(\lambda)$, it is checked that the eddy size is smaller than the bubble diameter. If so, the range of diameter for a daughter bubble is calculated based on mass, force and energy balance criteria. For the mass balance criterion, it is based on common sense that the daughter bubble cannot be larger than the parent bubble. The energy balance criterion is obtained from the balance of eddy kinetic energy and surface creation energy as follows:

$$\rho_l V_\lambda \frac{\bar{u}_\lambda^2}{2} \geq \pi d_1^2 \sigma + \pi d_2^2 \sigma - \pi d^2 \sigma = c_f \pi d^2 \sigma \quad \text{or}$$

$$d_1 \leq \sqrt{\frac{\rho_l V_\lambda \frac{\bar{u}_\lambda^2}{2}}{c_f \pi \sigma}} \quad (30)$$

Breakup happens when the eddy has enough kinetic energy so that the energy is enough to create new interface area for the daughter bubbles. Here, $\bar{u}_\lambda = (2.0)^{0.5} (\varepsilon \lambda)^{\frac{1}{3}}$ [23, 24] is assumed. For the force balance criterion, balance between inertial force (dynamic pressure) and surface tension force (capillary pressure) is considered as follows:

$$\rho_l \frac{\bar{u}_\lambda^2}{2} \geq \frac{\sigma}{d_1} \quad \text{or} \quad \frac{\sigma}{\rho_l \frac{\bar{u}_\lambda^2}{2}} \leq d_1 \quad (31)$$

Luo and Svendsen's theory had only an energy criterion and it encountered an unphysical result such that tiny bubbles are created extensively compared to experiment since it does not have any restriction for the minimum bubble size. To improve this model, Wang

et al. (2003) [21] added the minimum bubble size from the force balance criterion above.

By combining all three criteria, we get

$$d_{min} \leq d_1 \leq d_{max} \text{ or } \frac{\sigma}{\rho_l \frac{u_\lambda^2}{2}} \leq d_1 \leq \min(d, \sqrt{\frac{\rho_l V_\lambda \frac{u_\lambda^2}{2}}{c_f \pi \sigma}}) \quad (32)$$

Since the daughter bubble must satisfy all three criteria, the smaller upper bound is chosen for the maximum diameter among the energy and mass criteria. If the upper bound is greater than the lower bound, it means there is a daughter bubble size that satisfies all three criteria. Then, a bubble size is randomly picked in the diameter range with the uniform probability density function [25]. The diameter of another daughter bubble is then calculated after subtracting the first bubble volume from the parent bubble volume.

NUMERICAL MODEL SETUP FOR BENCHMARK TEST PROBLEM

Based on measurements by Hibiki et al (2001) [3], a vertical acrylic resin pipe with 50.8mm diameter (D) and 3.061m length test section is considered in this work as a test problem for the EEDPM model. This test section is chosen as the model domain (Z=0 is the domain inlet at the bottom, and Z=60.3D is the domain outlet at the top, which is assumed to be close to the outlet of the experimental system itself, so is set to 1atm pressure). Measurements of velocity of both phases, gas fraction and bubble size were

taken on two measurement planes, $Z=6D$ and $53.5D$. By assuming axisymmetric flow, a 1/6th sector of a pipe is used for the 3D domain, using a 42,000 hexahedral mesh. Because the incompressible EE models cannot account for gas expansion and the corresponding increase in gas fraction and velocity with distance up the pipe, the inlet velocity and gas fraction are specified as constants to match the average experimental data at the outlet measurement plane from Hibiki et al. (2001). Table 1 shows the inlet boundary conditions of the three cases modeled in this study.

Cases 1 and 2 are typical bubbly flows, and case 3 is in a transition between a bubbly and a slug flow regime. DPM bubbles are injected at $Z=6D$, based on the measured bubble sizes at that plane with gas flow rates taken from measurements at $Z=6D$, and inlet pressure from the EE model. The injection point (r, θ) on the cross-section of $Z=6D$ is randomly determined for each bubble as follows:

$$r = \frac{D}{2} \times \sqrt{R}, \theta = \frac{\pi}{3} \times R \quad (33)$$

where R is a uniform probability density function that varies from 0 to 1. These distribution functions make a uniform distribution on a fan-shape cross-sectional area. Once the injection point is determined, the injected bubble size is determined by the radial bubble size distribution from measurement data ($\bar{d}_{32} = \bar{d}_{32}(r)$). Instead of using the Sauter-mean bubble size \bar{d}_{32} from the measurement directly, a Rosin-Rammler size distribution is assumed for the injected bubble sizes.

$$d = \bar{d}_{32} \times \left(\ln \left(\frac{1}{1-R} \right) \right)^{\frac{1}{\delta}} \quad (34)$$

where $\delta = 4$, \bar{d}_{32} is from the measurement on Z=6D associated with the randomly determined radial injection point r , R is a uniform probability density function that varies from 0 to 1. The pipe wall is assumed to be a smooth wall, and a no-slip boundary condition is used for the liquid while a free-slip boundary condition is used for the gas. A wall function for single phase turbulent flow is applied for the liquid at the pipe wall. For DPM bubbles, a reflection boundary condition is applied at the wall. Elastic collisions are assumed when the distance from the wall becomes smaller than the bubble radius. This boundary condition is important to estimate an accurate bubble size near the wall since the DPM model allows a bubble to approach the wall until its center hits the wall. Side faces of the 1/6th sector of the pipe are prescribed as symmetric boundary conditions.

For the EE model and the EE part of the EEDPM model outlet, constant pressure boundary condition ($P = 1$ atmosphere pressure) is assumed at the outlet of the domain. For turbulence modeling, the SST $k - \omega$ model is used, which transitions from $k - \varepsilon$ in the bulk to $k - \omega$ near the wall through a blending function, as described elsewhere [10-11]. A time step of 0.001 second is chosen, based on satisfying the CFL number condition. Radial Sauter mean bubble size distributions are calculated from vertically integrated DPM bubbles in five equally-divided zones in height and the transiently-updated radial bubble size distributions ($d=d(r)$) are used for the EE model momentum interaction calculation of each zone. Velocity, gas fraction and bubble size distribution on the Z=53.5D plane are compared to the measurements. The new hybrid model is implemented in the commercial software ANSYS-Fluent through new user-defined (UDF) subroutines.

EE MODEL RESULTS WITH TOMIYAMA LIFT FORCE

First, the standard Eulerian-Eulerian model is used with a constant bubble size to simulate the three cases. The original Tomiyama lift force model is used to calculate the lift force [14]. Cases 1 and 2, in the bubbly flow regime, have nearly equal gas fractions, but case 2 has twice the Reynolds number of case 1 for both phases. The average bubble sizes measured on the measurement plane $Z=53.5D$ are 2.6mm for case 1, and 3.0mm for case 2. It was observed in the experiments that small bubbles ($d<3.6\text{mm}$) moved toward the wall due to the lift force and caused peaks of gas fraction and bubble diameter at $\sim 2.5\text{mm}$ from the wall.

Figure 2 shows velocity, gas fraction and local bubble size distribution profiles at $Z=53.5D$ for case 1. We observe a reasonable agreement with the experiment data, because the local bubble sizes do not deviate much from the average prescribed input bubble size of 2.6mm used in the simulation.

Figure 3 shows the same comparisons for case 2. These results under-estimate the velocities in the core region for both phases. The gas fraction peak near the wall is over-estimated slightly.

Figure 4 shows the same comparisons for case 3. The experiments observed that in case 3 the flow regime transitions from a bubbly flow to a slug flow. The big bubbles created by the coalescence process migrate toward the center of the pipe and cause a high gas fraction and large bubble sizes near the center. Due to the significant change of bubble size in the radial direction, the average bubble size of 4.0 mm cannot adjust the local bubble size properly. This causes a large deviation of the velocity magnitudes from

the measurements. The gas fraction profiles are completely different. The simulations show a wall-peak profile, but measurements show a core-peak profile. One reason for this disagreement is the lift force model. The Tomiyama lift force estimates a critical bubble size for the inversion of force direction as 5.8mm, so the lift force acts towards the wall for the 4.0mm bubbles.

EE MODEL RESULTS WITH MODIFIED LIFT FORCE

To improve the lift force calculation, a modified lift force model is used to re-compute case 3. Before doing that, the radially-varying bubble size distribution from the measurement at $Z=53.5D$ is used everywhere along the pipe instead of a constant averaged bubble size of 4.0mm. Figure 5 shows the EE model results, with the original Tomiyama lift model. Even though the bubble size distribution is imposed to match the measurements, there is still great disagreement of the velocity and gas fraction profiles.

On the other hand, the simulation results are improved when the modified lift model is used, as shown in Figure 6. Velocity profiles show reasonable agreement with the measurements, and the gas fraction correctly shows a core-peak profile. This result implies that modification of the lift force is necessary when there is a transition of flow regime from bubbly to slug flow in multi-bubble situations. Also, the EE model has potential to accurately simulate the transition regime when a proper bubble size distribution is provided.

EEDPM model results

We next recomputed cases 2 and 3 using the new EEDPM model including changes to the bubble size due to coalescence, break up and volumetric expansion. These bubble sizes are then used to compute the interactions between the bubble and the liquid phase. Figure 7 and 8 show two snapshots of bubble distributions, illustrating two bubbles coalescing and another bubble breaking up into two bubbles.

Figure 9 (left) shows the DPM bubble sizes at $Z=53.5D$ for case 2. In spite of the low gas fraction, collisions between bubbles happened and the coalescence effect on the bubble size distribution was not negligible. Modeling of elastic bounce after non-coalescing collisions is crucial to get a realistic bubble motion and spatial distribution of bubbles since the DPM model does not otherwise have a mechanism to avoid overlapping of bubbles. Unrealistic accumulation of DPM bubbles at the wall was observed due to the lift force if the elastic bounce effect is not included. A few breakups are observed near the wall, caused by the high turbulent dissipation rate which decreases the Sauter mean diameter near the wall.

Figure 10 shows Sauter-mean diameters of DPM bubbles at several locations for case 2 and compares them with the measurements. The injected DPM bubbles at $Z=6D$ plane increase in size due to both volumetric expansion and coalescence as they float upwards in the duct. It is seen that the Sauter-mean diameter of the DPM bubbles passing through $Z=53.5D$ plane matches the measurements well. The Sauter mean diameter profile obtained from vertically integrating over the DPM bubbles in the zone including $Z/D=53.5$ shows a similar trend to the results at $Z=53.5D$ but produces a slightly rough

bubble size distribution because it is a spatial average of bubbles in the zone at simulation time $t=18$ seconds. This radial bubble size distribution is transferred to the EE model for the calculation of momentum interactions at each time step at each zone.

Figure 11 shows the velocity and gas fraction from the EEDPM model and compares them with the measurements. The newly-computed velocity fields agree better with the experiment and are higher near the center, but the gas fraction is over-estimated near the center, and under-estimated near the wall compared to the measurements and to the pure EE model results shown in Fig 3. This error in gas fraction is due to an under-estimation of the lift coefficient by the modified lift force model. This suggests that a more sophisticated lift model is needed to simulate the effect of neighbor bubbles in the case of multiple bubbles.

Figure 12 shows the distribution of Sauter-mean diameters of the EEDPM bubbles for case 3 at different axial locations compared with the measurements. As shown in Figure 9 (right), the bubble size increases significantly near the center of the pipe due to the coalescence effect. Large bubbles ($d>3.6\text{mm}$) migrate toward the center by the lift force and create even larger bubbles through coalescence. On the other hand, breakup of bubbles near the wall creates smaller bubbles and causes a decrease in Sauter mean bubble diameter. The Sauter mean diameters obtained by the DPM model at $Z=53.5D$ matches well with the measurements. Figure 13 compares the velocity and gas fraction distributions with measurements. Compared to the results of the EE model presented in Figure 4, the EEDPM model shows a better agreement.

EVALUATION OF BUBBLE INTERACTION AND EXPANSION EFFECTS

To understand the importance of different contributions to the size change of bubbles quantitatively, parametric studies of case 2 and 3 are conducted by numerically activating only some of the effects, which include bubble collisions, volumetric expansion, breakup, and coalescence. Table 2 lists the activated effects in each run. The collision effect is always activated to avoid the unphysical overlapping of DPM bubbles.

Figure 14 and 15 show the comparison of these effects for case 2. It turned out that the coalescence effect is larger than the expansion effect in spite of the low gas fraction ($\alpha \cong 6\%$), and both effects are not negligible. Increase of the Sauter mean diameter from $Z=6D$ to $Z=53.5D$ by coalescence was 13.1%, compared to 7.0% by expansion. The total average increase in diameter from $Z=6D$ to $Z=53.5D$ was 18.9%. Especially, the coalescence effect is important to capture the peak near $r/R \cong 0.95$. Decrease of the Sauter mean diameter by breakup averaged 2.8%. The breakup effect is small and decreases average bubble sizes mostly near the wall.

Figure 16 and 17 display the comparison of the effects in case 3. The coalescence effect is dominant compared to other effects due to the higher gas fraction ($\alpha \cong 27\%$). The computed results with collision and coalescence roughly match the measurements at $Z=53.5D$. The total increase of Sauter mean diameters from $Z=6D$ to $Z=53.5D$ of 30.0% consisted of 20.6% from coalescence and 10.9% by expansion. Decrease of the Sauter mean diameter by breakup was negligible. From the comparison with case 2, while the volumetric expansion effect is determined mostly by height (both absolute height and

height difference) and initial bubble size, the coalescence effect depends greatly on local flow conditions.

CONCLUSIONS

A new hybrid EEDPM model for gas-liquid multiphase flow in gas-liquid systems has been developed and is tested for three cases of upward bubbly flow. The EEDPM model gives improved results compared to the EE model with a constant bubble size in both the bubbly flow regime (case 1 & 2) and the transition regime (case 3). This is due to improved calculation of the local bubble size distribution, which evolves dynamically space and time by coalescence, breakup and volumetric expansion, using a modified lift force relation and coalescence efficiency of 0.01. Further work is needed to improve the internal models for lift force and coalescence efficiency. The parametric studies of bubble interactions and volumetric expansion in case 2 and 3 show that the coalescence effect is larger than other effects, and the importance is dependent on the flow conditions such as the gas fraction.

ACKNOWLEDGMENT

The authors are thankful for the support from the Continuous Casting Consortium at the University of Illinois at Urbana-Champaign, and the US National Science Foundation (Grant CMMI 15-63553).

NOMENCLATURE

C_D	drag coefficient
C_L	lift coefficient
C_{WL}	wall lubrication coefficient
C_{TD}	turbulent dispersion coefficient
$C_{\mu,l}$	empirical constant of turbulence model
D	pipe diameter, m
d	bubble diameter, m
\bar{d}_{32}	Sauter mean diameter, m
E_o	Eotvos number
\mathbf{F}	force, N
\mathbf{g}	gravity acceleration, m/s^2
h_i	initial film thickness, m
h_f	final film thickness, m
K_{kq}	momentum transfer coefficient from phase k to q
k	turbulent kinetic energy, m^2/s^2
m_b	mass of bubble, kg
\mathbf{n}_w	unit normal wall vector
n_λ	number density of turbulent eddy, $1/\text{m}^3$
p	pressure, Pa

R	a uniform probability density function that varies from 0 to 1
F	cumulative probability density function
r	radial position in a pipe, m
Re_p	particle Reynolds number
t	Time, s
\mathbf{u}	velocity field, m/s
u	velocity magnitude, m/s
\bar{u}_λ	turbulent eddy velocity, m/s
\mathbf{v}_i	i-th DPM bubble velocity, m/s
V	volume, m ³
\mathbf{x}	DPM bubble position, m
y_w	distance from a wall, m
α	volume fraction
μ	viscosity, Pas
ρ	density, kg/m ³
σ	surface tension coefficient, N/m
ε	turbulent dissipation rate, m ² /s ³
λ	turbulent eddy size, m
η	Kormogolov eddy scale, m

Γ	gamma function
δ	parameter of Rosin-Rammler distribution
θ	angular position in a pipe

SUBSCRIPTS

B	buoyancy
b	bubble
c	computational cell
G	gravity
D	drag
di	i-th detached bubble
eq	equivalent
g	gas phase
i	i-th DPM bubble
L	lift
l	liquid phase
max	maximum
min	minimum
new	new position
old	old position

P	pressure gradient
T	turbulent dispersion
t	turbulence
V	virtual mass
W	wall lubrication
λ	turbulent eddy
1	a smaller bubble in a pair
2	a larger bubble in a pair

REFERENCES

- [1] Harlow, F. H., and Amsden, A. A., 1975, "Numerical Calculation of Multiphase Fluid Flow," *J Comput Phys*, 17(1), pp. 19–52.
- [2] Riley, J. J., 1974, "Diffusion Experiments with Numerically Integrated Isotropic Turbulence," *Phys Fluids*, 17(2), p. 292.
- [3] Hibiki, T., Ishii, M., and Xiao, Z., 2001, "Axial Interfacial Area Transport of Vertical Bubbly Flows," *Int J Heat Mass Tran*, 44(10), pp. 1869–1888.
- [4] Hulburt, H. M., and Katz, S., 1964, "Some Problems in Particle Technology," *Chem Eng Sci*, 19(8), pp. 555–574.
- [5] Lo, S., AEAT -1096, AEA Technology, 1996
- [6] Krepper, E., Lucas, D., Frank, T., Prasser, H. M., and Zwart, P. J., 2008, "The Inhomogeneous MUSIG Model for the Simulation of Polydispersed Flows," *Nucl Eng Des*, 238(7), pp. 1690–1702.
- [7] Ishii, M., and Hibiki, T., 2006, *Thermo-Fluid Dynamics of Two-Phase Flow*. Springer Science+Business Media, New York.
- [8] Riley, J. J. "Diffusion Experiments with Numerically Integrated Isotropic Turbulence." *Phys Fluids*, 17, no. 2 (1974): 292.
- [9] Rani, S. L., Winkler, C. M., and Vanka, S. P., 2004, "Numerical Simulations of Turbulence Modulation by Dense Particles in a Fully Developed Pipe Flow," *Powder Technol*, 141(1–2), pp. 80–99.
- [10] Yang, H. and Thomas, Brian G., 2017 "Multiphase flow and bubble size distribution in continuous casters using a hybrid EEDPM model", *Steel/SIM2017*, Paper No. SteelSim2017-en-42
- [11] Rzehak, R., and Kriebitzsch, S., 2015, "Multiphase CFD-Simulation of Bubbly Pipe Flow: A Code Comparison," *Int J Multiphas Flow*, 68, pp. 135–152.
- [12] Frank, Th., and Menter, F.R., 2003, ANSYS Germany internal report
- [13] Tomiyama, A., Kataoka, I., Zun, I., and Sakaguchi, T., 1998, "Drag Coefficients of Single Bubbles under Normal and Micro Gravity Conditions.," *JSME International Journal Series B*, 41(2), pp. 472–479.

- [14] Tomiyama, A., Tamai, H., Zun, I., and Hosokawa, S., 2002, "Transverse Migration of Single Bubbles in Simple Shear Flows," *Chem Eng Sci*, 57(11), pp. 1849–1858.
- [15] Hosokawa, S., Tomiyama, A., Misaki, S., and Hamada, T., 2002, "Lateral Migration of Single Bubbles Due to the Presence of Wall," *ASME 2002 Joint US-European Fluids Engineering Division Conference*, pp. 855–860.
- [16] Burns, A. D. B., Frank, Th., Hamill, I., and Shi, J.-M., 2004, "The Favre Averaged Drag Model for Turbulent Dispersion in Eulerian Multi-Phase Flows," *Fifth International Conference on Multiphase Flow, ICMF-2004*, paper No. 392
- [17] ANSYS Fluent Theory guide release 14.5. ANSYS Inc.
- [18] Auton, T. R., 1987, "The Lift Force on a Spherical Body in a Rotational Flow," *J Fluid Mech*, 183(1), p. 199.
- [19] Prince, M. J., and Blanch, H. W., 1990, "Bubble Coalescence and Break-up in Air-Sparged Bubble Columns," *AIChE J*, 36(10), pp. 1485–1499.
- [20] Luo, H., and Svendsen, H. F., 1996, "Theoretical Model for Drop and Bubble Breakup in Turbulent Dispersions," *AIChE J*, 42(5), pp. 1225–1233.
- [21] Wang, T., Wang, J., and Jin, Y., 2003, "A Novel Theoretical Breakup Kernel Function for Bubbles/Droplets in a Turbulent Flow," *Chem Eng Sci*, 58(20), pp. 4629–4637.
- [22] Nambiar, D. K. R., Kumar, R., Das, T. R., and Gandhi, K. S., 1992, "A New Model for the Breakage Frequency of Drops in Turbulent Stirred Dispersions," *Chem Eng Sci*, 47(12), pp. 2989–3002.
- [23] Kuboi, R., Komazawa, I., and Otake, T., 1972, "Behavior of Dispersed Particles in Turbulent Liquid Flow," *J Chem Eng Jpn*, 5(4), pp. 349–355.
- [24] Kuboi, R., Komazawa, I., and Otake, T., 1972, "Collision and Coalescence of Dispersed Drops in Turbulent Liquid Flow," *J Chem Eng Jpn*, 5(4), pp. 423–424.
- [25] Hesketh, R. P., Etchells, A. W., and Russell, T. W. F., 1991, "Experimental Observations of Bubble Breakage in Turbulent Flow," *Ind Eng Chem Res*, 30(5), pp. 835–841.

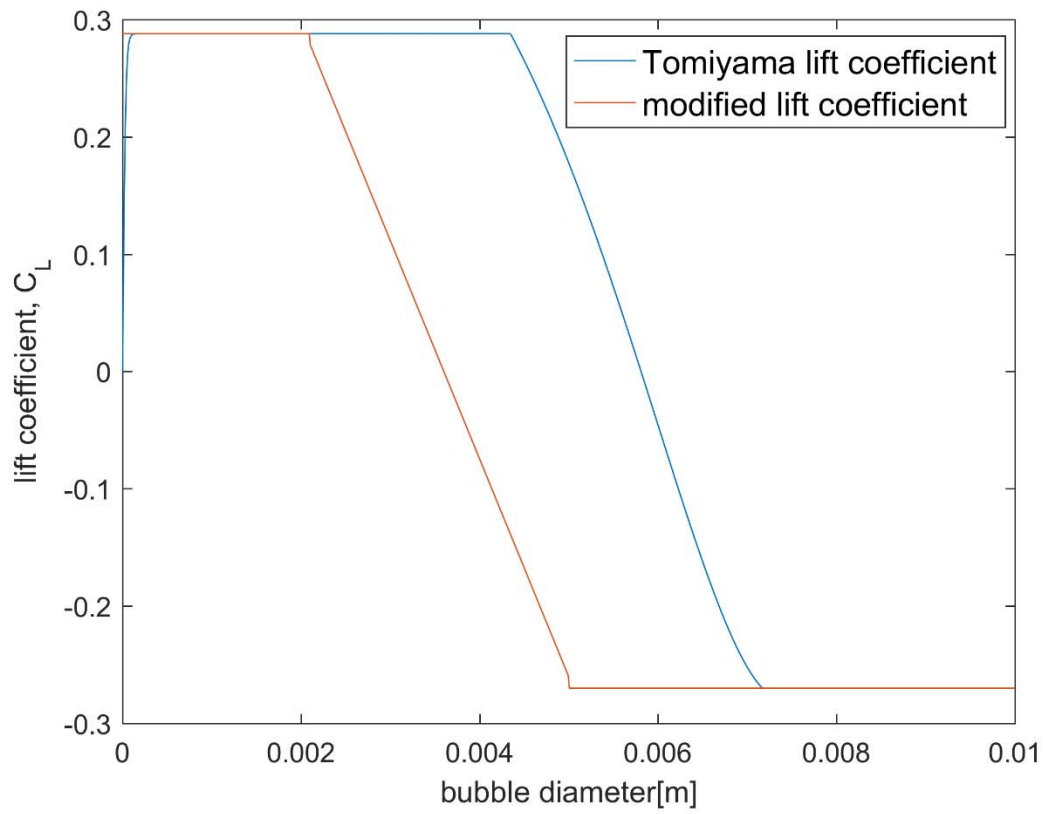


Figure 1

Fig. 1 Lift coefficient of Tomiyama model and a modified model

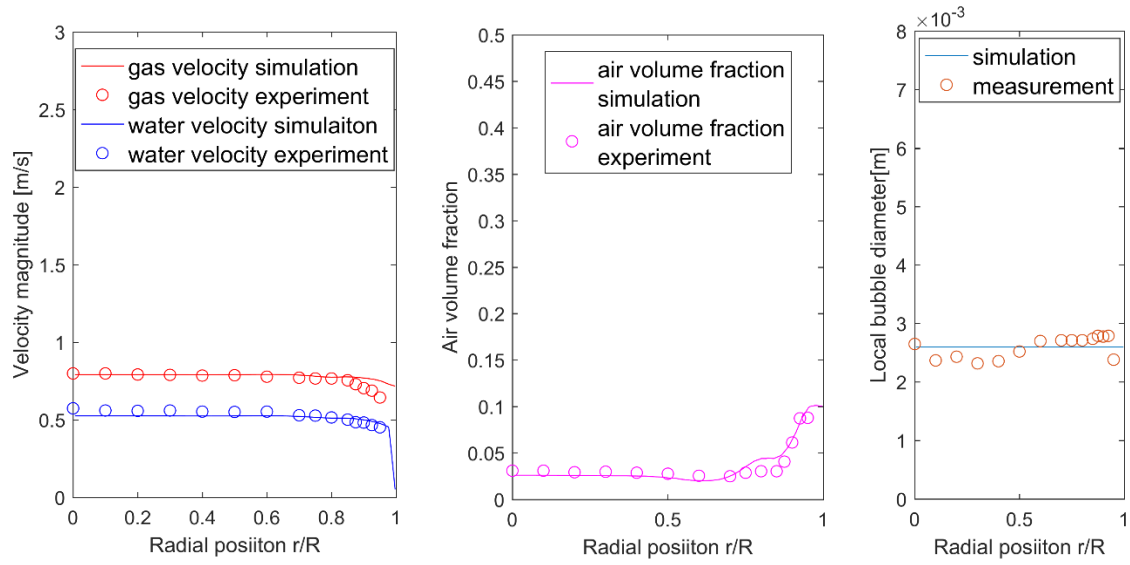


Figure 2

Fig. 2 Comparison of velocity, gas fraction and bubble size profiles at $Z=53.5D$ between measurements and EE simulation of case 1

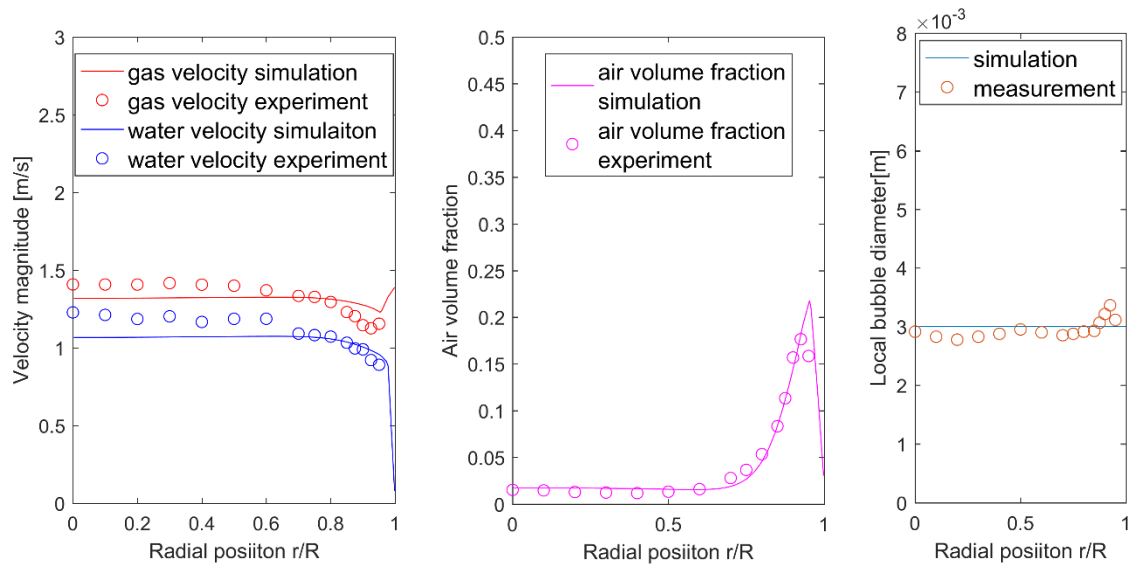


Figure 3

Fig. 3 Comparison of velocity, gas fraction and bubble size profiles at $Z=53.5D$ between measurements and EE simulation of case 2

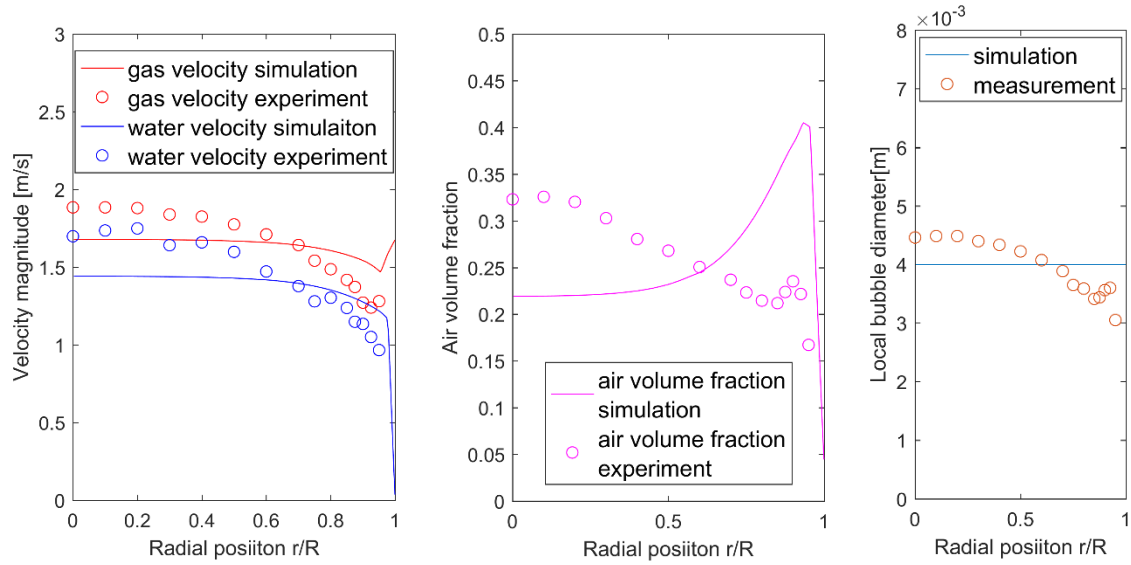


Figure 4

Fig. 4 Comparison of velocity, gas fraction and bubble size profiles at $Z=53.5D$ between measurements and EE simulation of case 3

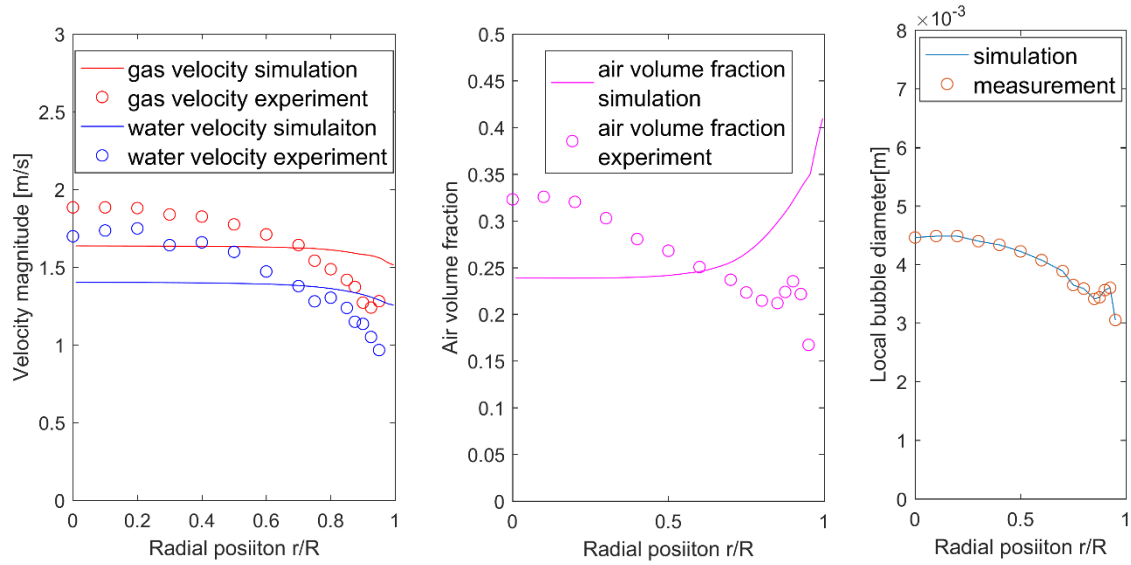


Figure 5

Fig. 5 Comparison of velocity, gas fraction and bubble size profiles at $Z=53.5D$ for EE simulation of case 3 with Tomiyama lift

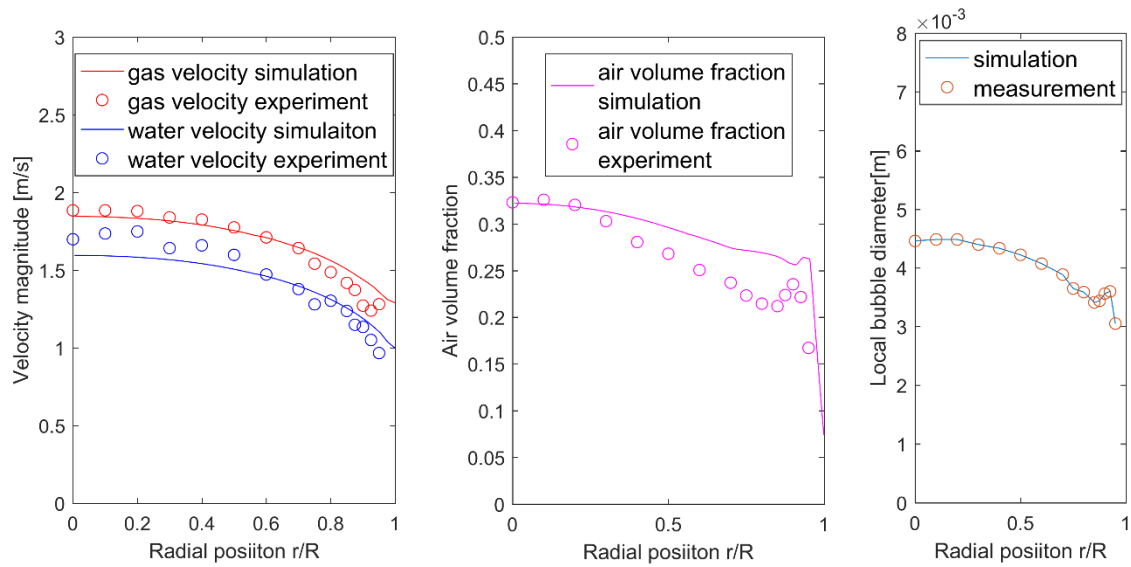


Figure 6

Fig. 6 Comparison of velocity, gas fraction and bubble size profile at $Z=53.5D$ for EE simulation of case 3 with modified lift

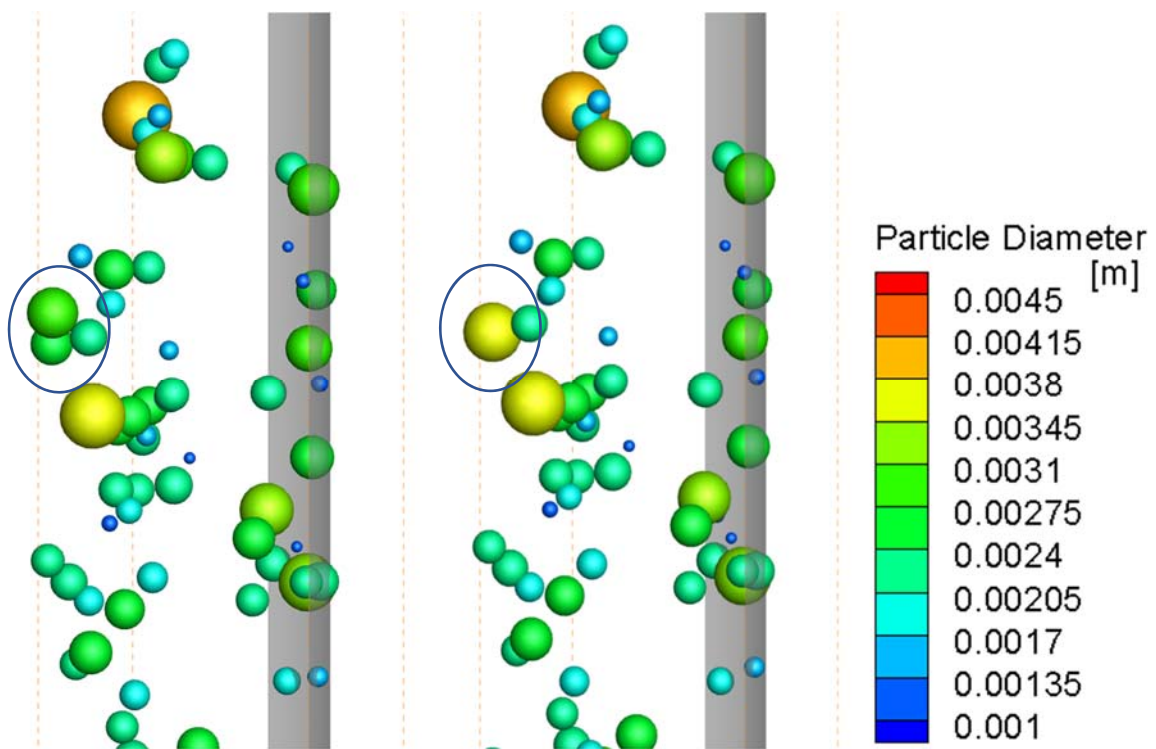


Figure 7

Fig. 7 Coalescence of bubbles naer the center of the pipe

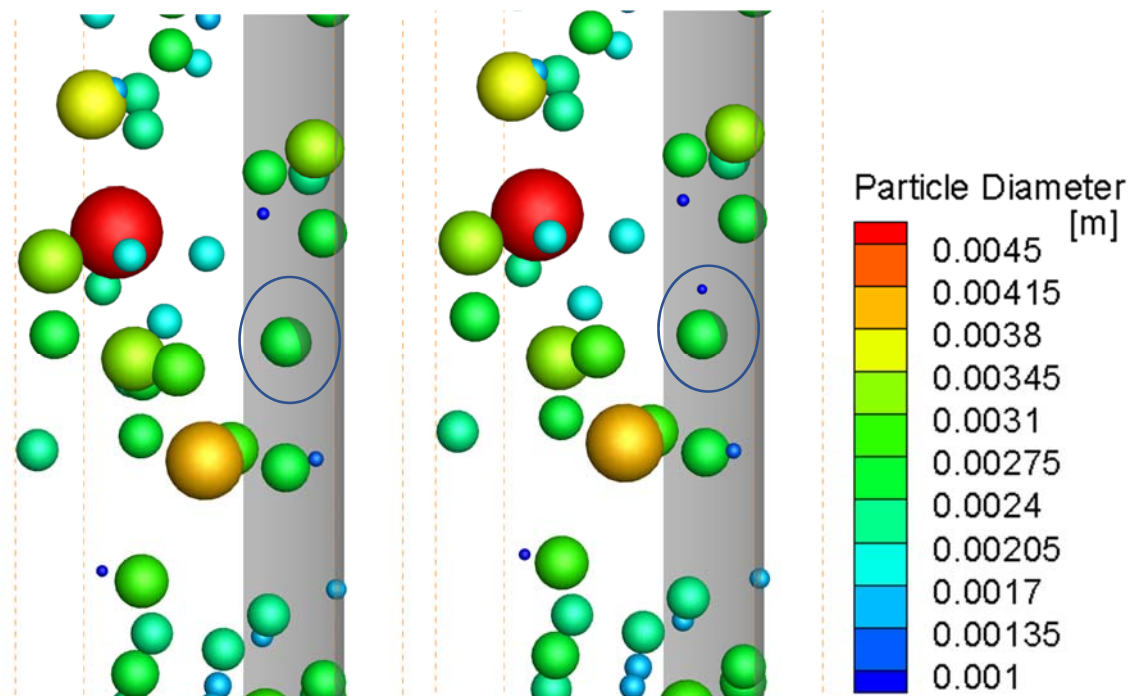


Figure 8

Fig. 8 Breakup of bubbles naer the wall

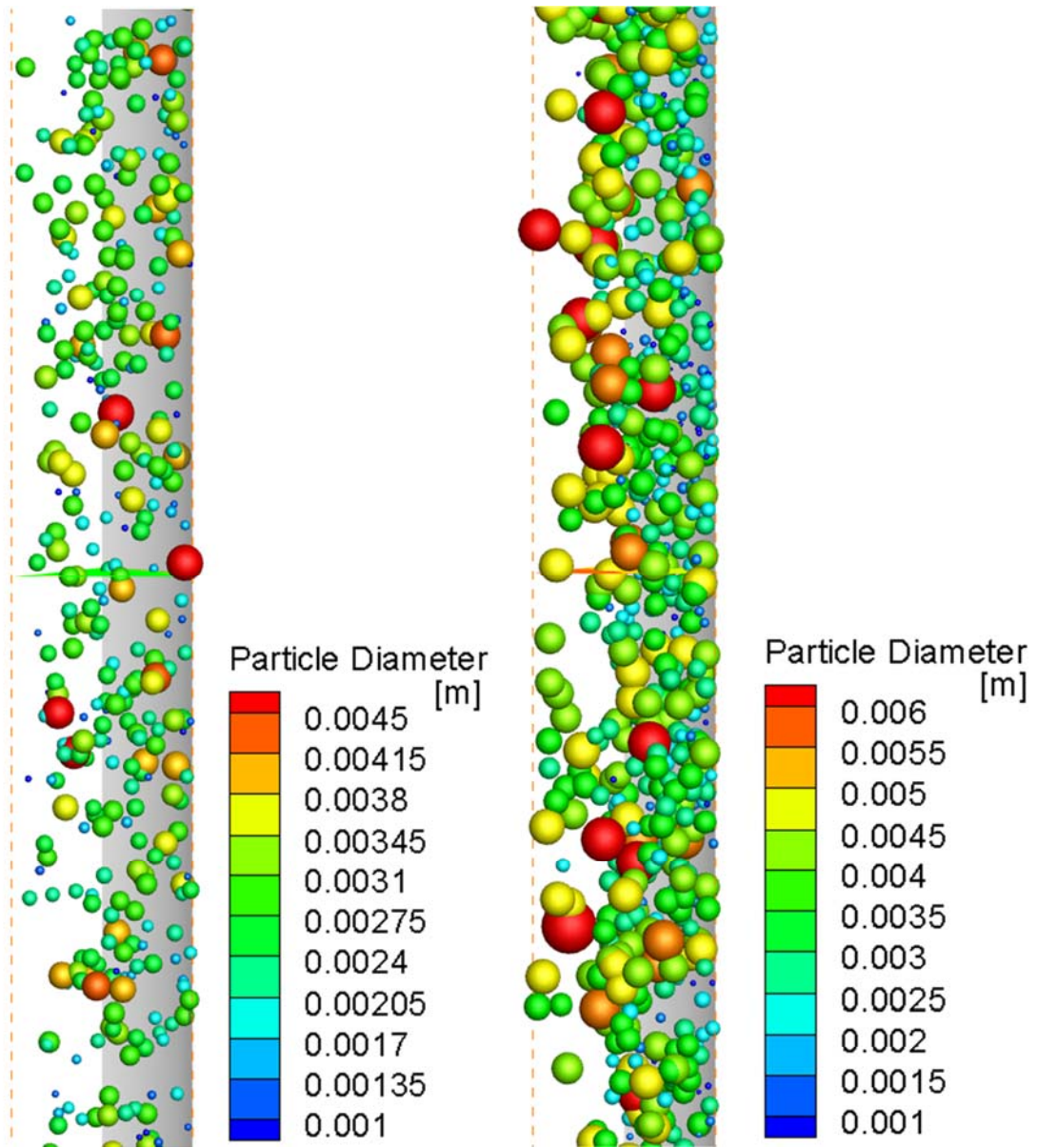


Figure 9

Fig. 9 DPM bubble distributions of case 2(left) and case 3(right) near Z=53.5D

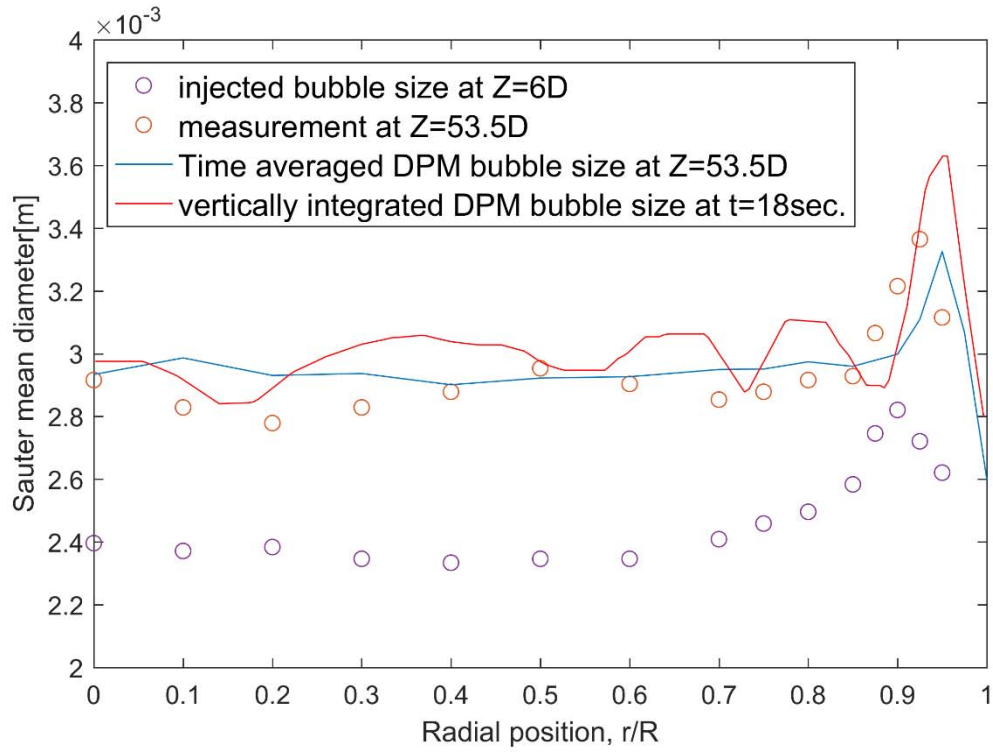


Figure 10

Fig. 10 Profiles of Sauter-mean diameter (case 2) of DPM bubbles from EEDPM at Z=6D, Z=53.5D and vertical integration, compared with measurements

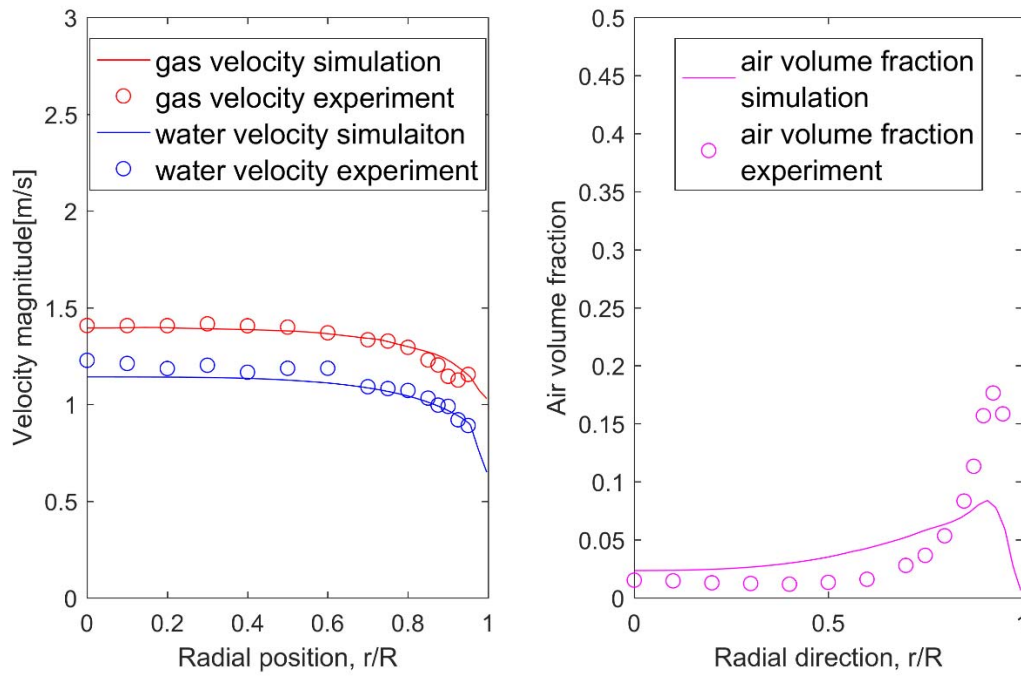


Figure 11

Fig. 11 Velocity and gas fraction profiles (case 2) from EEDPM at Z=53.5D and comparisons with measurements

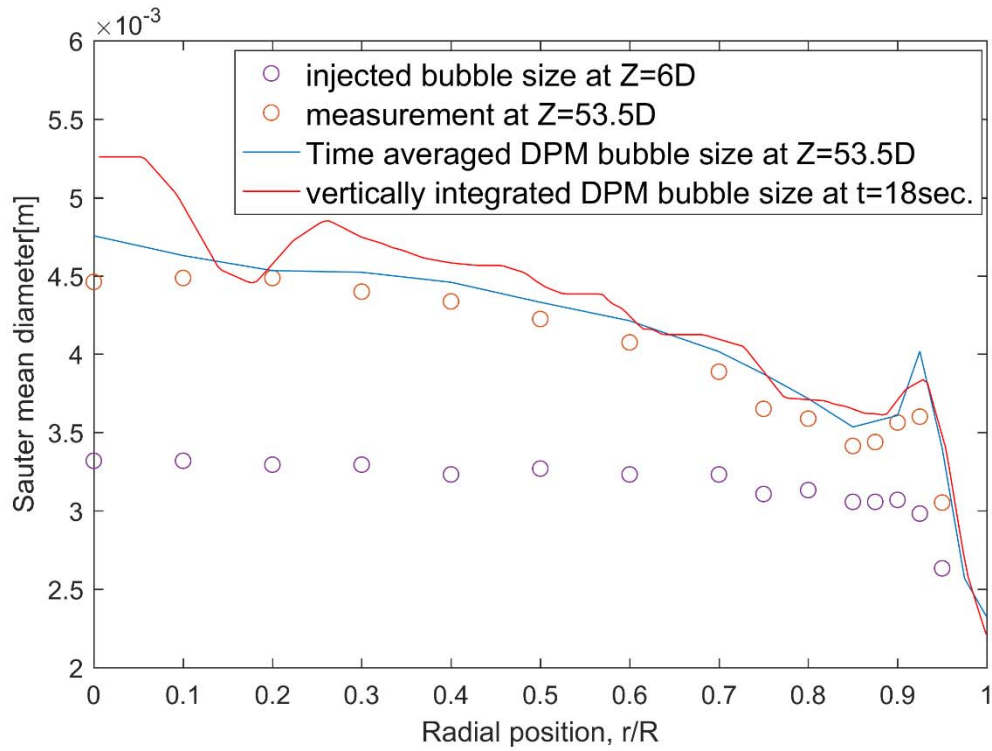


Figure 12

Fig. 12 Profiles of Sauter-mean diameter (case 3) of DPM bubbles from EEDPM at Z=6D, Z=53.5D and vertical integration, compared with measurements

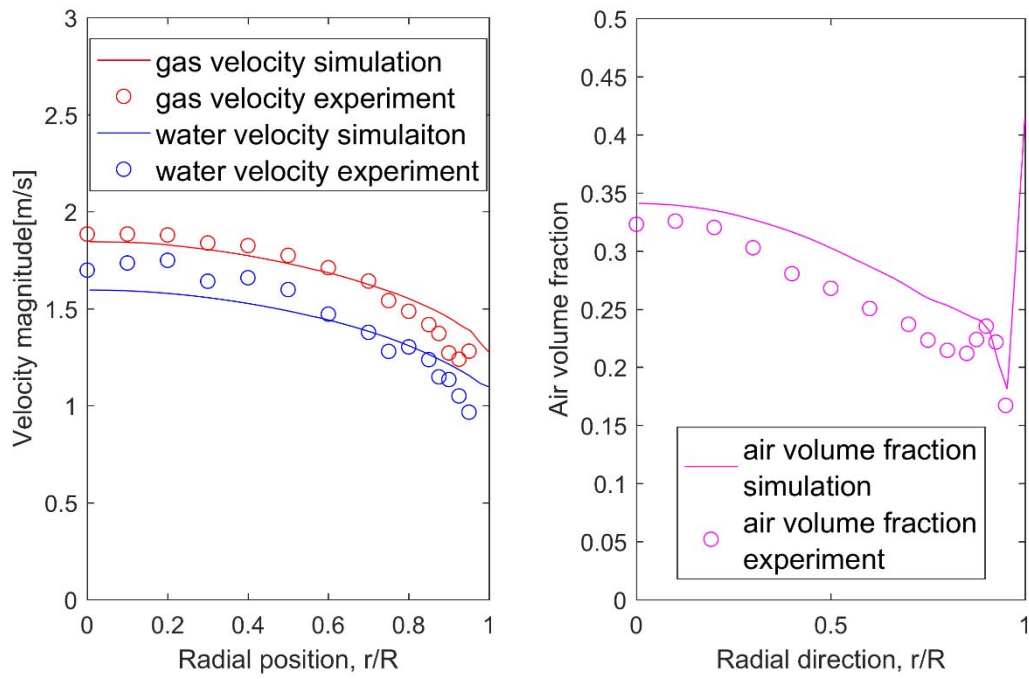


Figure 13

Fig. 13 Velocity and gas fraction profiles (case 3) from EEDPM at Z=53.5D and comparisons with the measurements

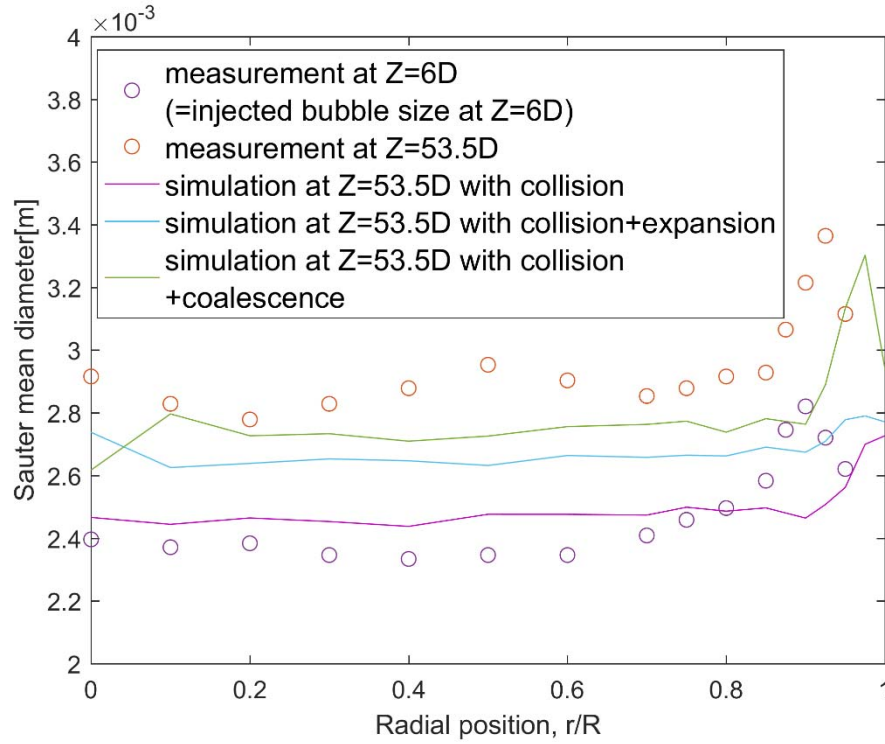


Figure 14

Fig. 14 Comparison of DPM bubble sizes from EEDPM at $Z=53.5D$ about run 1~3 for case 2

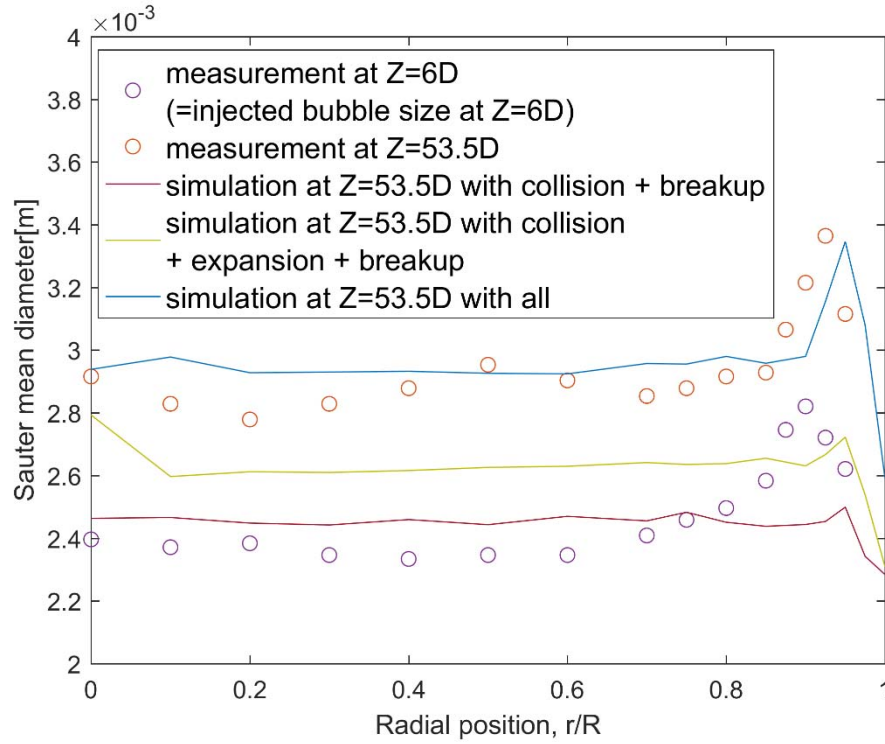


Figure 15

Fig. 15 Comparison of DPM bubble sizes from EEDPM at Z=53.5D about run 4~6 for case 2

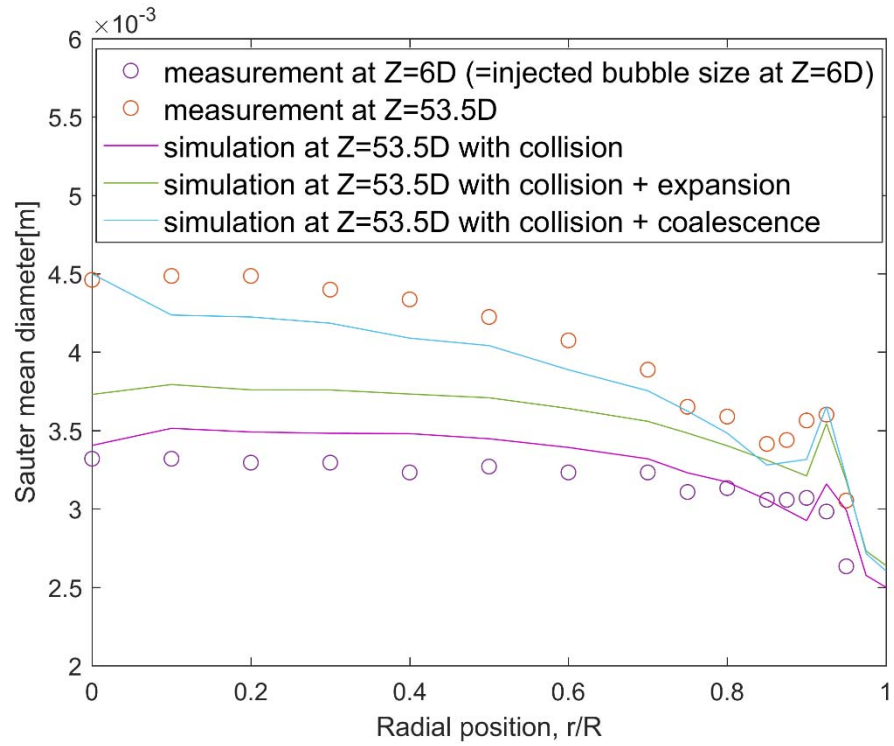


Figure 16

Fig. 16 Comparison of DPM bubble sizes from EEDPM at $Z=53.5D$ about run 1~3 for case 3

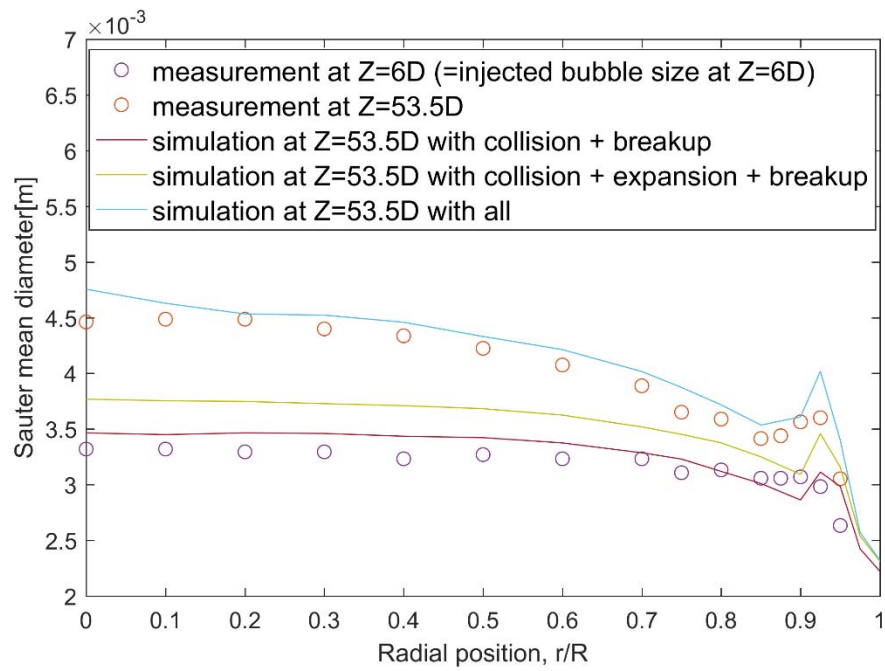


Figure 17

Fig. 17 Comparison of DPM bubble sizes from EEDPM at Z=53.5D about run 4~6 for case 3

Table 1

Table 1 Experimental conditions used in the simulation

Operating condition	Case 1	Case 2	Case 3
Water superficial velocity	0.491 m/s	0.986 m/s	0.986 m/s
Air superficial velocity	0.030 m/s	0.070 m/s	0.445 m/s
Gas fraction	4.14 %	5.75 %	26.96 %
Water velocity at inlet	0.512 m/s	1.046 m/s	1.350 m/s
Air velocity at inlet	0.734 m/s	1.217 m/s	1.650 m/s

Table 2

Table 2 The activated effects in each case of the parametric study

	collision	expansion	coalescence	breakup
Run 1	Yes	No	No	No
Run 2	Yes	Yes	No	No
Run 3	Yes	No	Yes	No
Run 4	Yes	No	No	Yes
Run 5	Yes	Yes	No	Yes
Run 6	Yes	Yes	Yes	Yes